This article has been accepted for publication in a future issue of this journal, but has not been fully edited. Content may change prior to final publication. Citation information: DOI 10.1109/JSEN.2015.2477444, IEEE Sensors Journal

Tightly-Coupled Integration of WiFi and MEMS Sensors on Handheld Devices for Indoor Pedestrian Navigation

Yuan Zhuang and Naser El-Sheimy

***Abstract*— The need for indoor pedestrian navigators is quickly increasing in various applications over the last few years. However, indoor navigation still faces many challenges and practical issues, such as the need for special hardware designs and complicated infrastructure requirements. This paper originally proposes a pedestrian navigator based on tightly-coupled (TC) integration of low-cost MEMS (micro-electromechanical systems) sensors and WiFi for handheld devices. Two other approaches are proposed in this paper to enhance the navigation performance: 1) The use of MEMS solution based on PDR/INS (pedestrian dead reckoning / inertial navigation system) integration; 2) The use of motion constraints, such as non-holonomic constraints (NHC), zero velocity update (ZUPT), and zero angular rate update (ZARU) for the MEMS solution. There are two main contributions in this paper: (1) TC fusion of WiFi, INS, and PDR for pedestrian navigation using an EKF (Extended Kalman Filter); and (2) Better heading estimation using PDR and INS integration to remove the gyro noise which occurs when only vertical gyroscope is used. The performance of the proposed navigation algorithms has been extensively verified through field tests in indoor environments. Experiment results showed that the average RMS position error of the proposed TC integration solution was 3.47m in three trajectories, which is 0.01% of INS, 10.38% of PDR, 32.11% of the developed MEMS solution, and 64.58% of the loosely-coupled (LC) integration. The proposed TC integrated navigation system can work well in the environment with sparse deployment of WiFi access points (APs).**

***Index Terms*— Tightly-coupled integration, indoor pedestrian navigation, MEMS sensors, WiFi, motion constraints.**

I. INTRODUCTION

IN the past several years, the demand for handheld devices such as smartphones has grown exponentially. Multi-applications, such as calling, texting, gaming, and internet browsing, make smartphones essential tools for people's everyday life. Technological advancements have facilitated the manufacturing of compact, inexpensive, and low-power consuming receivers and sensors for smartphones, therefore, enabling the development of smartphone-based pedestrian navigation applications. Smartphones create limitless possibilities for navigation and positioning applications due to their sophisticated microprocessors, powerful operating systems, embedded sensors, and portable characteristics.

Yuan Zhuang and Naser El-Sheimy are with the University of Calgary, 2500 University Drive, NW, Calgary, AB, T2N 1N4, Canada. (E-mail: zhuangy@ucalgary.ca; elsheimy@ucalgary.ca).

GPS, which is usually embedded in smartphones, provides an accurate position solution outdoors [1] [2]. However, the degradations and interruptions of GPS signals mean that GPS cannot be used to achieve accurate and continuous navigation solutions in challenging areas such as urban canyons, tunnels, and indoors [3] [4] [5]. On the other hand, the demand for indoor navigation is quickly increasing in various applications including: health care monitoring, logistics, Location Based Services (LBS), emergency services, tourism, and people management [6] [7] [8]. Indoor pedestrian navigation has been a popular research topic in the last decade [9].

This paper proposes an indoor pedestrian navigator based on tightly-coupled (TC) integration of low-cost MEMS sensors and WiFi. In order to make the smartphone-based navigator accurate and practical, three methods are proposed in this paper to enhance the navigation performance: 1) The use of the MEMS solution based on PDR/INS (pedestrian dead reckoning / inertial navigation system) integration; 2) The use of non-holonomic constraints (NHC), zero velocity update (ZUPT), and zero angular rate update (ZARU) for the MEMS solution; 3) The use of advanced TC integration for MEMS and WiFi (i.e., TC fusion of INS, PDR, and WiFi).

The first approach improves the indoor pedestrian navigation solution based on smartphones through the use of PDR/INS integration for the MEMS solution. MEMS sensors are usually used as either INS or PDR for pedestrian navigation. To the best of our knowledge, almost none of the previous work combine them for pedestrian navigation. The paper uses a PDR/INS-integrated MEMS solution, which was originally proposed in [10], to combine the advantages of both schemes. In this algorithm, step detection and step length estimation are kept the same as the traditional PDR algorithm. The estimated step length is then used to calculate the forward speed, which works as the velocity update for the INS to limit the velocity error, and further limit the position and attitude errors. Therefore, the PDR/INS-integrated MEMS solution is better than the INS stand-alone solution. The heading from the PDR/INS integration also performs better when compared with PDR because it considers the effect of the roll and pitch.

The second improvement is due to the use of motion constraints, such as NHC, ZUPT, and ZARU for the MEMS

This article has been accepted for publication in a future issue of this journal, but has not been fully edited. Content may change prior to final publication. Citation information: DOI 10.1109/JSEN.2015.2477444, IEEE Sensors Journal

solution. NHC considers the fact that a land vehicle cannot move horizontal sideways or vertically to work as the velocity update to improve the MEMS solution [3]. It is also suitable for normal pedestrian walking. ZUPT uses the zero velocity as the velocity update to limit the velocity error if the pedestrian is static [11]. ZARU considers the fact that the heading is unchanging to limit the attitude error if the pedestrian is static [12]. With these motion constraints, the indoor pedestrian navigator is expected to provide a better navigation solution.

The third approach originally uses the TC integration of WiFi and MEMS to improve the navigation performance of handheld devices. The proposed TC integration integrates the raw data of MEMS sensors with WiFi-RSS-based (Received Signal Strength) distances/ranges. Fifteen states for MEMS (3D position error, 3D velocity error, 3D attitude error, gyroscope drift, and accelerometer bias) and 1 state (the bias of the WiFi Received Signal Strength (RSS)) for WiFi are used as the state vector in the EKF (Extended Kalman Filter) for the TC integration. The main benefit of this method is that the drift of MEMS sensors can be reduced by WiFi even if only one or two access points (APs) are available. The introduction of the WiFi RSS bias in the TC integration also improves the performance of the proposed system.

The rest of the paper is organized as follows. In Section II, literature review is discussed. Next, the system overview is presented in Section III. In Section IV, the proposed MEMS solution is described. The TC integration of MEMS and WiFi is presented in Section V and experimental results are presented in Section VI. Finally, the conclusions and future work are summarized in Section VII.

II. Literature Review

Several researches have been conducted for the integration of WiFi and MEMS sensors [13-17]. The research [13] proposes a pedestrian navigation algorithm based on the integration of WiFi and foot-mounted inertial sensors. In most cases, foot-mounted systems are not as convenient as handheld systems. An integration method is proposed in [14] for MEMS sensors and a fingerprinting-based WiFi positioning solution. However, WiFi fingerprinting requires labor-cost survey for the radio map database. [15] reports a particle filter for the integration of WiFi and inertial sensors. The large computation load of the particle filter makes it unsuitable for running on smart devices. [16] reports the results of the integration of MEMS sensors and ToF-based (Time of Flight) WiFi ranges. The limitation of this work is that ToF is not supported by current WiFi chipsets. [17] improves the navigation performance of the integration of low-cost sensors and WiFi in smartphones by realizing cooperative positioning among multiple pedestrians. The proposed method introduces linkage structures to simplify trajectories of pedestrians. Meanwhile, these structures work as a constraint to reduce the number of variables to be estimated. In addition, a new navigation algorithm is proposed in [18] to fuse the WiFi RSS values and inertial sensor data from smartphones. A sequential Monte Carlo filter is developed for inertial sensor based tracking, and a radiolocation algorithm is developed to infer mobile location based on RSS measurements. Almost all current WiFi/MEMS integrations are loosely-coupled (LC) integrations, which means that the integration is based on MEMS navigation solution and WiFi positioning solution.

On the other hand, the TC integration has been used for the integration of inertial sensors with GPS, RFID (Radio-frequency Identification), and USBL (Ultra-Short Baseline) [12, 19-23]. [19] and [20] report the results of GPS/INS TC integration by using non-linear filters for land vehicle applications. The work of [21] uses GPS/INS TC integration for UAV applications. The Kalman Filter (KF) is used in the TC integration. [22] proposes a TC integration of GPS and INS for missile applications. A TC integration of UBSL and INS is proposed in [23] for underwater vehicles. Meanwhile, [12] reports a TC integration for INS and RFID for pedestrians in indoor environments. The limitation of this work is that some RFID hardware needs to be installed before the navigation. To the best of our knowledge, none of TC integration for WiFi and MEMS sensors has been proposed and assessed before. This paper fills this gap of current researches.

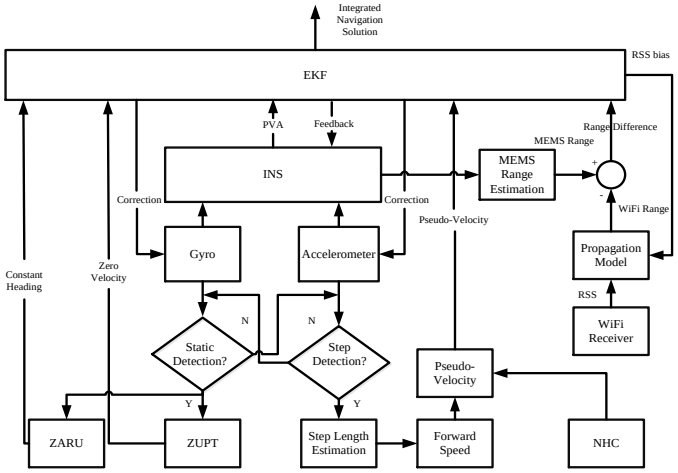

Fig. 1. Block diagram of the proposed indoor pedestrian navigator based on the TC integration of MEMS sensors and WiFi.

III. System Overview

The block diagram of the proposed TC WiFi/MEMS integration for indoor pedestrian navigation is shown in Fig. 1. The proposed system mainly includes three main modules: the MEMS solution based on the PDR/INS integration and motion constraints, WiFi-based range estimation, and EKF-based TC integration. In the proposed MEMS solution, data from gyroscopes and accelerometers are first passed to the INS mechanization. The accelerometer and gyroscope data are also used for step detection and static detection, respectively. If the step detection succeeds and the static detection fails, PDR step length is estimated in the module of "step length estimation", and is further used to derive the forward speed. NHC is also used to constrain the lateral and vertical speeds of the moving platform. The PDR-based forward speed and the NHC-based lateral and vertical speeds are combined to 3-axis pseudo-velocity to work as the velocity update for the INS to limit the velocity error. If the step detection fails and static detection succeeds, ZUPT and ZARU apply zero velocity and

This article has been accepted for publication in a future issue of this journal, but has not been fully edited. Content may change prior to final publication. Citation information: DOI 10.1109/JSEN.2015.2477444, IEEE Sensors Journal

unchanging heading as the velocity and heading updates for the INS to reduce navigation errors. Finally, this MEMS solution is used to generate the MEMS-based range information. In WiFi-based range estimation, RSS values from the handheld devices pass to the propagation model to generate the range information. In the part of EKF-based TC integration, range differences between MEMS-based ranges and WiFi-based ranges pass to the EKF to estimate the state vector errors. The estimated state vector errors (3D position, velocity, and attitude errors; accelerometer bias, gyroscope drift; and WiFi RSS bias) are fed back to the INS and WiFi range estimation. After the feedback, INS outputs the final integrated navigation solution for pedestrians indoors.

IV. Sensor-Based Navigation

A. INS-based Navigation

INS mechanization is typically implemented for the inertial navigation. The accelerations and angular rates from accelerometers and gyroscopes are used in the INS mechanization to compute the 3D position, 3D velocity, and 3D attitude of the moving object [24]. The INS mechanization equations are given as follows [11]:

$$\begin{bmatrix} \dot{r}^n \\ \dot{v}^n \\ \dot{C}_b^n \end{bmatrix} = \begin{bmatrix} D^{-1}v^n \\ C_b^n f^b - (2\Omega_{ie}^n + \Omega_{en}^n)v^n + g^n \\ C_b^n(\Omega_{ib}^b - \Omega_{in}^b) \end{bmatrix} \quad (1)$$

where $r^n = [\phi \quad \lambda \quad h]^T$ represents the position vector (latitude, longitude, and height), in which T represents the transpose for a vector; $v^n = [v_N \quad v_E \quad v_D]^T$ represents the velocity vector in the navigation frame; C_b^n represents the transformation matrix from the body frame to the navigation frame as a function of attitude components; g^n represents the gravity vector in the navigation frame; Ω_{ie}^n represents the skew-symmetric matrix of the rotation vector, ω_{ie}^n, from the navigation frame to the inertial frame; Ω_{en}^n represents the skew-symmetric matrix of the rotation vector, ω_{en}^n, from the navigation frame to the ECEF (Earth-Centered, Earth-Fixed) frame. $\Omega_{ib}^b, \Omega_{in}^b$ represent the skew-symmetric matrices of the gyroscope-based angular rate vector, ω_{ib}^b, and the rotation vector, ω_{in}^b, from the navigation frame to the inertial frame, respectively; and D^{-1} represents a 3×3 matrix related to the latitude, ϕ, and the ellipsoidal height, h, of the object.

B. PDR-based Navigation

The PDR determines a pedestrian's current position from the knowledge of the previous position and measurements of motion direction and traveled distance. The PDR algorithm usually includes step detection, step length estimation, heading estimation, and PDR mechanization [10] [25] [26]. In the step detection, steps are usually detected by means of the cycle pattern of the acceleration norm. Currently, peak detection, zero crossing, auto/cross correlation, and spectral analysis are typical approaches for the step detection [27]. In this paper, peak detection is used for the step detection.

"Step length estimation" is used to estimate the moving distance of the pedestrian at each step. Different practical models have been proposed for estimating the step length. In this paper, the practical model proposed in [28] is used to estimate step length, which assumes the step length is proportional to the vertical movement of the human hip. The largest difference of the vertical acceleration at each step is used to calculate vertical movement. The equation for step length estimation is expressed as

$$s = \sqrt[4]{a_{z\max} - a_{z\min}} \cdot K \quad (2)$$

where $a_{z\max}$ is the maximum value of the vertical acceleration, a_z. $a_{z\min}$ is the minimum value of a_z; and K is a calibrated constant parameter.

With the assumption that the handheld device is level (roll and pitch are zero degrees), the pedestrian's moving direction (heading) is usually estimated through the integral of the vertical gyroscope. However, the assumption is incorrect sometimes, and affects the navigation performance. Therefore, a PDR-derived heading is not used in the proposed MEMS navigation solution. Finally, PDR mechanization is given by

$$\begin{aligned} E_k &= E_{k-1} + \hat{s}_{(k-1,k)} \cdot \sin(\hat{H}_k) \\ N_k &= N_{k-1} + \hat{s}_{(k-1,k)} \cdot \cos(\hat{H}_k) \end{aligned} \quad (3)$$

where (E_{k-1}, N_{k-1}) and (E_k, N_k) are the positions at epoch $k-1$ and epoch k, respectively. $\hat{s}_{(k-1,k)}$ and $\hat{H}_k$ are the estimated step length and heading at epoch k, respectively.

C. Extended Kalman Filter

The EKF is usually used to fuse other information to reduce the drift of MEMS-based navigation solution. It estimates the optimal state of a process by minimizing the mean of square errors [29]. The state vector is usually defined as

$$x_s = [\delta r_{1\times3} \quad \delta v_{1\times3} \quad \varepsilon_{1\times3} \quad d_{1\times3} \quad b_{1\times3}]^T \quad (4)$$

where δr, δv, and ε represent the errors of position, velocity, and attitude, respectively. $d_{1\times3}$ and $b_{1\times3}$ represent gyroscope drift and accelerometer bias, respectively, which are estimated and fed back to the INS mechanization. The discrete-time EKF system model and observation model can be expressed as

$$\begin{cases} \delta x_k = \Phi_{k-1,k}\delta x_{k-1} + \omega_k \\ \delta z_k = H_k \delta x_k + \upsilon_k \end{cases} \quad (5)$$

where δx_k and δz_k represent the state vector and observation misclosure vector at epoch k, respectively. $\Phi_{k-1,k}$ represents the state transition matrix from epoch $k-1$ to epoch k, and H_k represents the design matrix at epoch k. ω_k and υ_k represent the process noise and observation noise at epoch k, respectively. For more details about the implementation of EKF for integrated navigation systems, please refer to [29].

This article has been accepted for publication in a future issue of this journal, but has not been fully edited. Content may change prior to final publication. Citation information: DOI 10.1109/JSEN.2015.2477444, IEEE Sensors Journal

D. Integrated INS and PDR Sensor Navigation

INS and PDR are two main approaches for MEMS-based pedestrian navigation. As shown in (1), the INS-based navigation system provides a complete navigation solution (i.e., 3D position, 3D velocity, and 3D attitude), however, INS mechanization uses two integrals to obtain the position information, and one integral to get the attitude information [30]. The total INS mechanization has three integrals. In the INS mechanization, an accelerometer bias introduces a 1st order error in velocity and a 2nd order error in position, and a gyro bias introduces a 2nd order error in velocity and a 3rd order error in position [31]. Therefore, when using the INS mechanization, the positioning error is accumulated quickly for low-grade MEMS sensors in smart devices which usually have large accelerometer and gyro biases. The PDR mechanization is shown in (3), in which the estimation of the step length $\hat{s}_{(k-1,k)}$ does not have integrals, and the estimation of the heading $\hat{H}_k$ has one integral. The total PDR mechanization only has one integral, which is much less than the INS. Therefore, PDR drifts much slower than INS, and provides a more accurate navigation solution. However, if the roll and pitch effects cannot be ignored, the PDR heading will be inaccurate since it is derived from the direct integral of the vertical gyroscope [32].

In this paper, a more robust MEMS solution is used based on the PDR/INS integration and motion constraints. In the proposed MEMS solution, the MEMS raw data is first processed by the INS mechanization. Next, these data is used to detect the moving status of the pedestrian. If the pedestrian is detected as "static", ZUPT and ZARU are used as updates for the INS to improve the navigation solution. On the contrary, PDR-based forward speed and NHC-based lateral and vertical speeds are combined to form the pseudo-velocity, which works as the 3D pseudo-velocity update for the INS to limit the velocity error.

TABLE I summarizes the motion detection and motion constraints used in this research. The status of the pedestrian is determined as "moving" or "static" when the corresponding conditions in TABLE I are satisfied. Then, the corresponding motion constraints are used to improve the navigation performance [10].

TABLE I
MOTION DETECTION AND MOTION CONSTRAINTS

Detected Motion Status	Conditions	Motion Constraints
Static	(1) The standard deviation of the angular rate norms during a certain time is less than the threshold (2) No steps are detected	ZUPT & ZARU
Moving	(1) The standard deviation of the angular rate norms during a certain time is larger than the threshold (2) Steps are detected	PDR/INS Integration (3D Pseudo-Velocity Update)

In the "static" case, the velocity misclosure in the body frame for ZUPT is given by [10]

$$\delta z = v_{INS}^b - v_{ZUPT}^b \tag{6}$$

where v_{ZUPT}^b represents the zero velocity vector. $v_{INS}^b = \left(C_b^n\right)^T \cdot v_{INS}^n$ represents the pedestrian velocity from the INS mechanization in the body frame, C_b^n represents the transformation matrix from the body frame to the navigation frame, and v_{INS}^n represents the pedestrian velocity from the INS mechanization in the navigation frame. The observation model for ZUPT is given by

$$\delta v^b = H_{v^b}\delta x + \upsilon_{v^b} \tag{7}$$

where υ_{v^b} represents the measurement noise. H_{v^b} represents the corresponding design matrix:

$$H_{v^b} = \begin{bmatrix} 0_{3\times3} & \left(C_b^n\right)^T & -\left(C_b^n\right)^T \cdot S\left(v^n\right) & 0_{3\times7} \end{bmatrix} \tag{8}$$

where $S\left(v^n\right)$ is the skew-symmetric matrix of v^n [11]. ZARU is also used in the "static" case, and the heading misclosure for ZARU is given by [10]

$$\delta z = \psi_{INS} - \psi_0 \tag{9}$$

where ψ_{INS} is the pedestrian heading from the INS mechanization, and ψ_0 is the pre-stored heading of the last epoch before the "static" was detected. The ZARU observation model is given by

$$\delta\psi = H_\psi \delta x + \upsilon_\psi \tag{10}$$

where υ_ψ represents the measurement noise; and H_ψ represents the design matrix:

$$H_\psi = \begin{bmatrix} 0_{1\times6} & \partial\psi/\partial\varepsilon_N & \partial\psi/\partial\varepsilon_E & \partial\psi/\partial\varepsilon_D & 0_{1\times7} \end{bmatrix} \tag{11}$$

For the details of $\partial\psi/\partial\varepsilon_N$, $\partial\psi/\partial\varepsilon_E$, and $\partial\psi/\partial\varepsilon_D$, please refer to [3].

In the "moving" case, with the assumption that the pedestrian's moving speed is constant for a short term, the forward speed is expressed in

$$v_f = s / t_s \tag{12}$$

where s represents the estimated step length and t_s represents the step time. Meanwhile, the lateral and vertical speeds of the pedestrian are constrained by the NHC. Therefore, the 3D pseudo-velocity vector in the body frame is given by [10]

$$v_{pseudo}^b = \begin{bmatrix} v_f & 0 & 0 \end{bmatrix}^T \tag{13}$$

Similar to ZUPT, this pseudo-velocity vector works as 3D pseudo-velocity update for INS to improve the pedestrian navigation performance.

V. TC INTEGRATION OF MEMS SENSORS AND WIFI

In this section, the TC integration of MEMS and WiFi is described in detail, including "MEMS-based range", "WiFi-based range", "system model of TC integration" and "observation model of TC integration". In this paper, WiFi-based ranges are calculated based on the WiFi propagation model. The main advantage of TC integration is that WiFi-based ranges can be used to aid MEMS in the case that less than three WiFi APs are observed, whereas LC integration cannot estimate the WiFi positions to aid the MEMS sensors in this case. The proposed TC WiFi/MEMS integration has better

This article has been accepted for publication in a future issue of this journal, but has not been fully edited. Content may change prior to final publication. Citation information: DOI 10.1109/JSEN.2015.2477444, IEEE Sensors Journal

performance than the LC integration, especially in the environment with a sparse deployment of WiFi APs.

A. MEMS-based Range

TC WiFi/MEMS integration involves the use of new measurement data, namely the MEMS-based range, given by

$$d_{MEMS,k}=\sqrt{\left[\left(\lambda_{MEMS}-\lambda_{AP,k}\right)\left(N+h\right)\cos\varphi_{MEMS}\right]^2+\left[\left(\varphi_{MEMS}-\varphi_{AP,k}\right)\left(M+h\right)\right]^2+\left(h_{MEMS}-h_{AP,k}\right)^2} \quad (14)$$

where λ_{MEMS}, φ_{MEMS}, and h_{MEMS} represent MEMS-based position coordinates (longitude, latitude, and altitude); $\lambda_{AP,k}$, $\varphi_{AP,k}$, and $h_{AP,k}$ represent position coordinates of the k^{th} WiFi AP (longitude, latitude, and altitude); M represents the meridian radius of the earth curvature; and N represents the prime vertical radius of the earth curvature.

B. WiFi-based Range

The typical propagation model follows the distance power law:

$$RSS=A-10\cdot n\cdot log_{10}(d)+X_\sigma \quad (15)$$

where RSS represents the received signal strength in dBm at a distance, d, from the transmitter. A represents a constant which depends on several factors: averaged fast and slow fading, transmitter gain, receiver gain, and transmitted power. Therefore, in practice, its value is usually unknown beforehand [33]. n represents the path loss exponent with typical values, 2 - 6 indoors. X_σ represents the shadow noise modeled as a Gaussian random variable with zero mean and standard deviation, σ_{RSS} [33] [34]. The range between the receiver and the transmitter can be estimated by the maximum likelihood estimator (MLE), and the result is given by [33]:

$$\hat{d}_{RSS}=10^{(A-RSS)/10\cdot n} \quad (16)$$

The experimental standard deviation of RSS values, σ_{RSS}, is almost independent of d [33]. By differentiating the propagation model in (15) with respect to d, we obtain

$$\frac{\partial RSS}{\partial d}=-\frac{10\cdot n}{\ln(10)\cdot d} \quad (17)$$

Therefore, the standard deviation of the range d is given by

$$\sigma_d=\ln(10)\cdot d\cdot\sigma_{RSS}/10\cdot n \quad (18)$$

where σ_d is linearly proportional to d, which illustrates the fact that the uncertainty of the range estimation grows with the range d. Note that there are other propagation models that consider the effects of walls and floors [35] [36]. However, they are not suitable for a real-time navigation system because a priori information of walls and floors are usually unavailable.

RSS measurements usually contain a bias for several reasons such as the inaccurate pre-set value of the constant A in (15). Therefore, the estimated range, $\hat{d}_{RSS}$, is not equal to the geometric range, d, between the transmitter and the receiver. The RSS bias, b_{RSS}, is considered to compensate the difference between $\hat{d}_{RSS}$ and d. Therefore, the geometric range is given by

$$d=10^{(A-RSS-b_{RSS})/10\cdot n}=10^{(A-RSS)/10\cdot n}\cdot 10^{-b_{RSS}/10\cdot n}=\hat{d}_{RSS}\cdot 10^{-b_{RSS}/10\cdot n} \quad (19)$$

By reorganizing (19), we obtain

$$\hat{d}_{RSS}=d\cdot 10^{b_{RSS}/10\cdot n}=d\cdot f\left(b_{RSS}\right) \quad (20)$$

where $f\left(b_{RSS}\right)=10^{b_{RSS}/10\cdot n}$. $f\left(b_{RSS}\right)$ is linearized at the point of $b_{RSS}=0$ by using the Taylor expansion, and the result is given by

$$\begin{aligned} f\left(b_{RSS}\right)&=f\left(0\right)+\frac{\partial f\left(b_{RSS}\right)}{\partial b_{RSS}}|_{b_{RSS}=0}\cdot b_{RSS}+\cdots \\ &\approx 1+\left(\ln 10/10\cdot n\cdot 10^{b_{RSS}/10\cdot n}\right)|_{b_{RSS}=0}\cdot b_{RSS} \\ &=1+\ln 10\cdot b_{RSS}/10\cdot n \end{aligned} \quad (21)$$

Substitute (21) into (20), we obtain the relationship between $\hat{d}_{RSS}$ and d:

$$\hat{d}_{RSS}=d+\left(\ln 10\cdot d/10\cdot n\right)b_{RSS} \quad (22)$$

In the TC WiFi/MEMS integration, the RSS bias b_{RSS} is also put in the state vector, and estimated by the EKF. Therefore, the system also can improve the estimation of WiFi-based range by the feedback of the estimated RSS bias, and further improve the navigation performance.

C. System Model of TC Integration

In the TC integration of MEMS and WiFi, error states in the EKF consist of two parts. The first part is the sensor error states. Its system dynamic equation is given as

$$\delta\dot{x}_s=F_s\delta x_s+G_s\omega_s \quad (23)$$

The sensor error state vector, δx_s, is given in (4). For the details about the dynamic matrix, F_s, please refer to [11]. $\omega_s=\left[\omega_1\ \cdots\ \omega_{15}\right]^T$, in which the elements comply with the assumptions of zero-mean and Gaussian distributed white noise and are uncorrelated with each other. Thus, the corresponding G_s is a unit matrix with a rank of 15.

The second part of the error states is the WiFi error state. In this research, WiFi RSS bias is used to compensate the error in the propagation model to estimate a more accurate range. WiFi RSS bias is modeled as a random walk process. The differential equation can be written as follows:

$$\dot{b}_{RSS}=\omega_{b_{RSS}} \quad (24)$$

where $\omega_{b_{RSS}}$ is the white noise. The WiFi system dynamic model is given by

$$\delta\dot{x}_W=F_W\delta x_W+G_W\omega_W \quad (25)$$

where $\delta x_W=b_{RSS}$, $F_W=0$, $G_W=1$, and $\omega_W=\omega_{b_{RSS}}$.

By combining (23) and (25), we have the following system model for the TC WiFi/MEMS integration.

This article has been accepted for publication in a future issue of this journal, but has not been fully edited. Content may change prior to final publication. Citation information: DOI 10.1109/JSEN.2015.2477444, IEEE Sensors Journal

$$\begin{bmatrix}\delta\dot{x}_s\\ \delta\dot{x}_W\end{bmatrix}=\begin{bmatrix}F_s & 0\\ 0 & F_W\end{bmatrix}\begin{bmatrix}\delta x_s\\ \delta x_W\end{bmatrix}+\begin{bmatrix}G_s & 0\\ 0 & G_W\end{bmatrix}\begin{bmatrix}\omega_s\\ \omega_W\end{bmatrix} \quad (26)$$

$$i.e.\ \ \delta\dot{x}=F\delta x+G\omega$$

D. System Model of TC Integration

The range differences between the WiFi-based ranges and the MEMS-based ranges are used as the observation vector, δz_d, in the TC EKF. By assuming there are m APs in-view, the measurements can be written as

$$\delta z_d=\begin{bmatrix}\delta z_{1,range}\\ \vdots\\ \delta z_{\mathrm{m},range}\end{bmatrix}=\begin{bmatrix}d_{MEMS,1}-d_{WiFi,1}\\ \vdots\\ d_{MEMS,\mathrm{m}}-d_{WiFi,\mathrm{m}}\end{bmatrix} \quad (27)$$

where $d_{MEMS,\mathrm{k}}$ is the MEMS-estimated range based on (14), and $d_{WiFi,\mathrm{k}}$ is the k^{th} AP's WiFi-based range measurement. Through (22), WiFi-based range of the k^{th} AP is given by

$$d_{WiFi,\mathrm{k}}=d_k+\left(\ln 10\cdot d_k \big/ 10\cdot n_k\right)b_{RSS}+\upsilon_{d_k} \quad (28)$$

where υ_{d_k} is the white noise of $d_{WiFi,\mathrm{k}}$. n_k is the path loss exponent for the k^{th} AP. d_k is the geometric range between the pedestrian and the k^{th} WiFi AP, which is expressed as

$$d_k=\sqrt{\left[\left(\lambda-\lambda_{AP,k}\right)\left(N+h\right)\cos\varphi\right]^2+\left[\left(\varphi-\varphi_{AP,k}\right)\left(M+h\right)\right]^2+\left(h-h_{AP,k}\right)^2} \quad (29)$$

where λ, φ, and h represent the filtered pedestrian's coordinates (longitude, latitude, and altitude); $\lambda_{AP,k}$, $\varphi_{AP,k}$, and $h_{AP,k}$ represent coordinates of the k^{th} WiFi AP (longitude, latitude, and altitude). By using the Taylor expansion for (29) and ignoring high-order errors, the range error model is given in

$$\delta d\approx e_k^T\cdot\begin{bmatrix}\delta\lambda & \delta\varphi & \delta h\end{bmatrix}^T+\left(\ln 10\cdot d_k \big/ 10\cdot n_k\right)b_{RSS} \quad (30)$$

where

$$e_k=\begin{bmatrix}e_{kx}\\ e_{ky}\\ e_{kz}\end{bmatrix}=\left(1+\ln 10\cdot b_{RSS} \big/ 10\cdot n_k\right)\begin{bmatrix}\left(\varphi-\varphi_{AP,k}\right)\left(M+h\right) \big/ d_k\\ \left(\lambda-\lambda_{AP,k}\right)\left(N+h\right)\cos\varphi \big/ d_k\\ h-h_{AP,k} \big/ d_k\end{bmatrix} \quad (31)$$

Therefore, the observation model for the range differences is given by

$$\delta z_d=\begin{bmatrix}d_{MEMS,1}-d_{WiFi,1}\\ \vdots\\ d_{MEMS,\mathrm{m}}-d_{WiFi,\mathrm{m}}\end{bmatrix}$$

$$=\begin{bmatrix}e_{1x} & e_{1y} & e_{1z}\\ \vdots & \vdots & \vdots\\ e_{mx} & e_{my} & e_{mz}\end{bmatrix}\begin{bmatrix}\delta\varphi\\ \delta\lambda\\ \delta h\end{bmatrix}+\begin{bmatrix}\ln 10\cdot d_1 \big/ 10\cdot n_1\\ \vdots\\ \ln 10\cdot d_m \big/ 10\cdot n_k\end{bmatrix}b_{RSS}+\begin{bmatrix}\upsilon_{d_1}\\ \vdots\\ \upsilon_{d_m}\end{bmatrix} \quad (32)$$

$$=G_{m\times 3}\begin{bmatrix}\delta\varphi & \delta\lambda & \delta h\end{bmatrix}^T+B_{m\times 1}\cdot b_{RSS}+\upsilon_{d,m\times 1}$$

Finally, the observation model for TC integration is written as

$$\delta z=H\delta x+\upsilon \quad (33)$$

where $\delta z=\delta z_d$ represents the measurement vector; $\upsilon=\upsilon_{d,m\times 1}$ represents the measurement noise vector; and H is the design matrix, which is expressed as

$$H=\begin{bmatrix}G_{m\times 3} & 0_{m\times 12} & B_{m\times 1}\end{bmatrix} \quad (34)$$

VI. Experimental Results

To evaluate the performance of the proposed indoor pedestrian navigator, several experiments were performed with three different Samsung Galaxy S III smartphones. Three pedestrians were involved in collecting field experiment data in different days. Smartphones that contain an accelerometer triad, a gyroscope triad, and a WiFi receiver were used to collect this data. Three experimental trajectories taken by separate pedestrians with various smartphones were in building E (about 120m * 40m) as shown in Fig. 2 (a), (b), and (c). In this experiment, 47 APs are used for positioning. The exact positions of these APs are unknown. However, their positions are estimated through a crowdsourcing method [6], and the result is marked in the floorplan. The numbers of observable WiFi APs in three tested trajectories are shown in Fig. 2 (d).

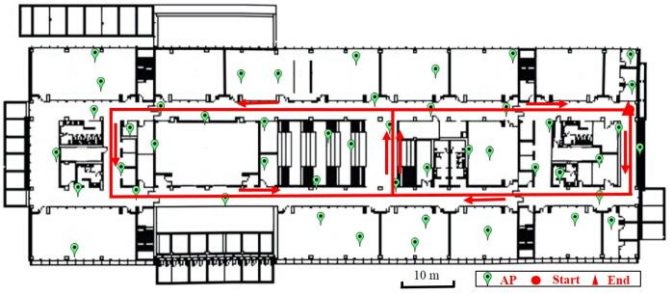

(a)

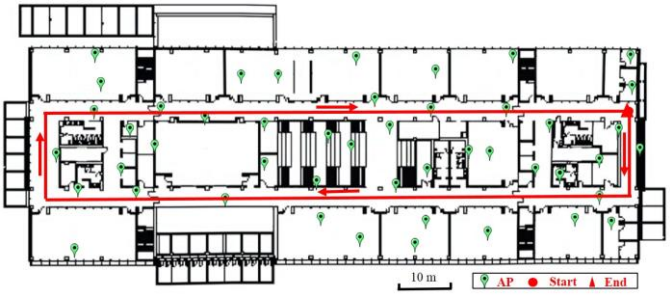

(b)

This article has been accepted for publication in a future issue of this journal, but has not been fully edited. Content may change prior to final publication. Citation information: DOI 10.1109/JSEN.2015.2477444, IEEE Sensors Journal

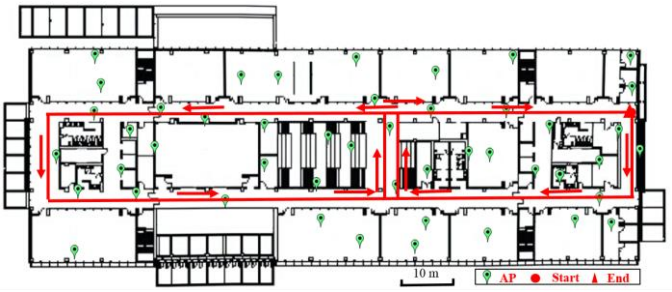

(c)

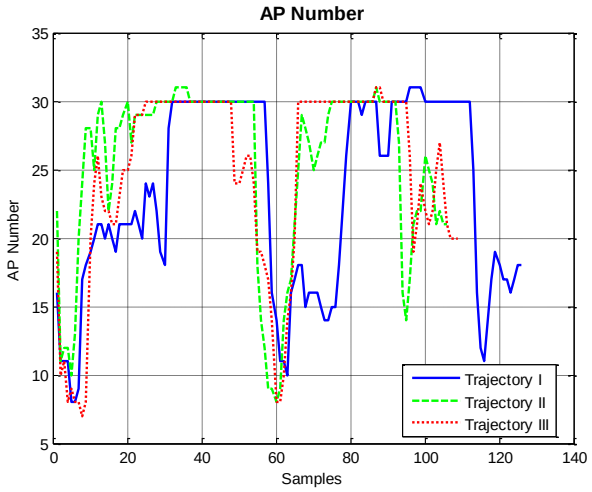

(d)

Fig. 2. Three experimental trajectories in building E (about 120 m × 40m): (a) Trajectory I, (b) Trajectory II, (c) Trajectory III, and (d) Observed AP numbers in the trajectories.

"Pedestrian 1" using "Smartphone A" performed the first experiment for nearly 5 minutes. The navigation solutions and error probabilities of different approaches in Trajectory I are shown in Fig. 3 and Fig. 4, respectively. The approaches used for navigation performance comparison include PDR, MEMS, LC WiFi/MEMS integration, and TC WiFi/MEMS integration. The proposed MEMS solution based on PDR/INS integration and motion constraints had an RMS (Root Mean Square) position error of 10.83m, which is better than the PDR RMS position error of 27.79m. The traditional INS navigation results are not depicted in Fig. 3 and Fig. 4 due to their large RMS position error of 13855.30m. This huge error is caused by the large noise characteristics of low-grade MEMS sensors in smartphones and the integrals used in the INS mechanization. The proposed TC WiFi/MEMS integration, using all observable APs, had a RMS position error of 3.72m, which is better than the RMS position error of the LC integration, which was 4.87m. This difference is due to the contribution of estimating the RSS bias. As shown in Fig. 3 and Fig. 4, navigation solutions of TC integrations, using two selected APs and one selected AP, are used to illustrate the performance of TC integration in the environment of the sparse deployment of WiFi APs. This showed RMS position errors of 5.77m and 5.87m, respectively. Their navigation performance was worse than the TC integration, which used all observable APs. However, they performed better than the proposed MEMS solution. The results illustrate that TC integration can improve the navigation performance of the MEMS solution, even if less than 3 APs are observed.

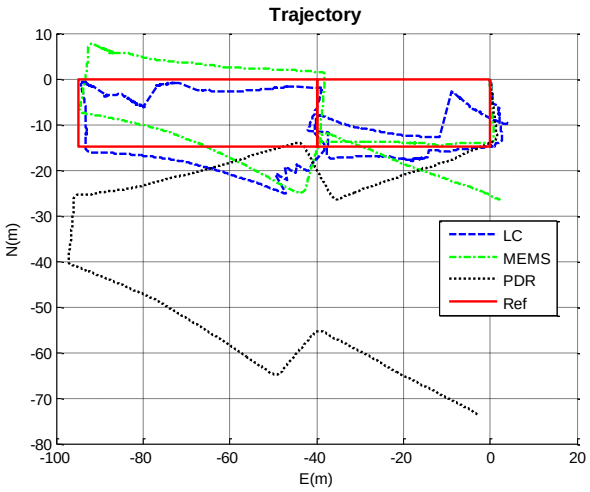

(a)

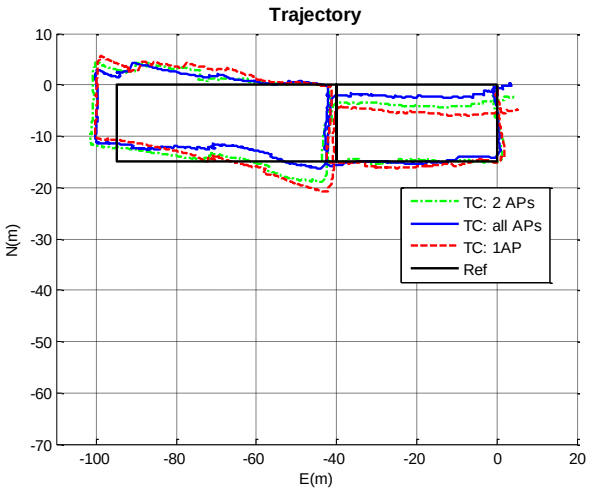

(b)

Fig. 3. Navigation solutions in Trajectory I (Pedestrian 1, Smartphone A). (a) PDR, MEMS, and WiFi/MEMS LC integration; and (b) WiFi/MEMS TC integration using different numbers of APs.

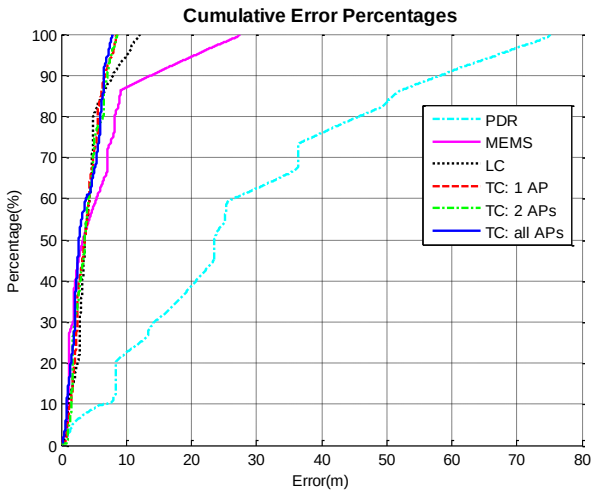

Fig. 4. Cumulative error percentages of PDR, MEMS, WiFi/MEMS LC integration and WiFi/MEMS TC integration using different numbers of APs in Trajectory I.

"Pedestrian 2" using "Smartphone B" performed the second experiment for about 4 minutes. The navigation solutions and error probabilities of different approaches in Trajectory II are

This article has been accepted for publication in a future issue of this journal, but has not been fully edited. Content may change prior to final publication. Citation information: DOI 10.1109/JSEN.2015.2477444, IEEE Sensors Journal

shown in Fig. 5 and Fig. 6, respectively. The proposed MEMS solution had a RMS position error of 11.02m, which is better than the PDR RMS position error of 34.00m. The proposed TC WiFi/MEMS integration, using all observable APs, had a RMS position error of 4.19m, which is slightly better than the 4.87m RMS position error of the LC integration. With two selected APs and one selected AP, TC integrations had RMS position errors of 4.36m and 4.44m, respectively. Like the first trajectory, their navigation performance was worse than the TC integration which used all observable APs. However, both the previous two cases had better navigation performance than in the proposed MEMS solution. The results also illustrate that TC integration can improve the navigation performance of the MEMS solution even if less than 3 APs are observed. These outcomes confirm the results of the first trajectory.

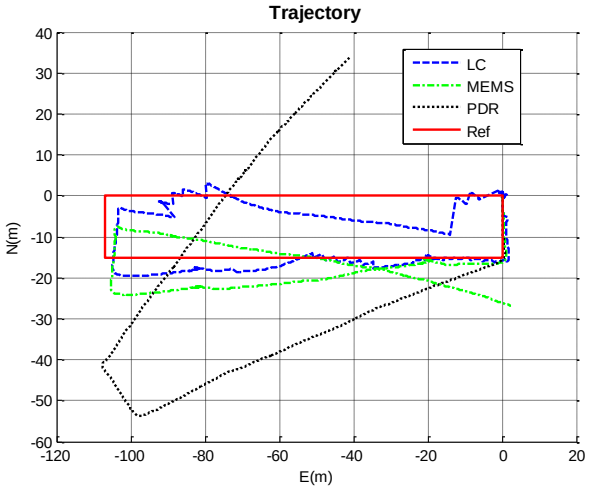

(a)

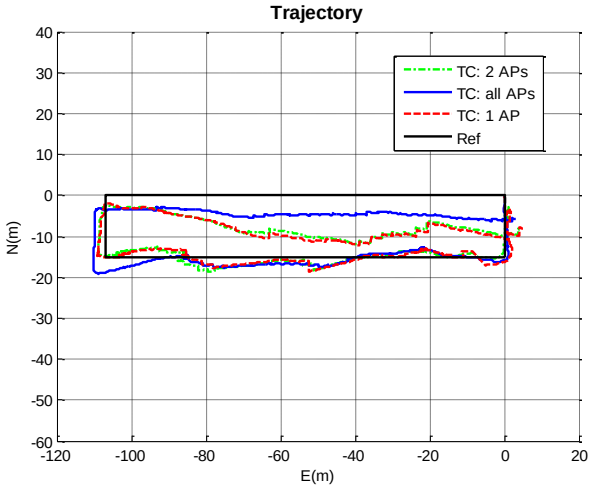

(b)

Fig. 5. Navigation solutions in Trajectory II (Pedestrian 2, Smartphone B). (a) PDR, MEMS, and WiFi/MEMS LC integration; and (b) WiFi/MEMS TC integration using different numbers of APs.

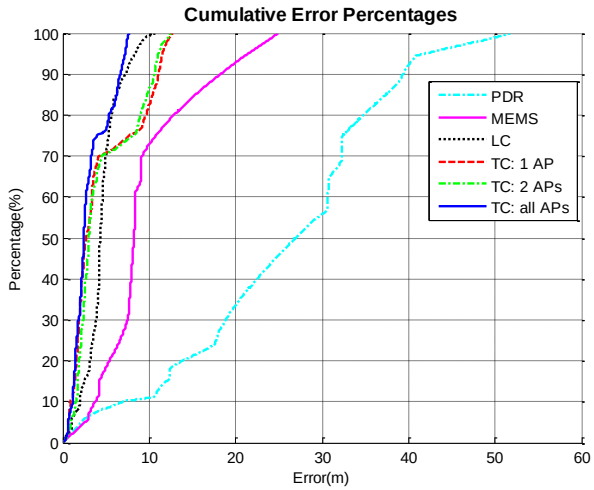

Fig. 6. Cumulative error percentages of PDR, MEMS, WiFi/MEMS LC integration and WiFi/MEMS TC integration using different numbers of APs in Trajectory II.

"Pedestrian 3" using "Smartphone C" performed the third experiment for approximately 5 minutes. The navigation solutions and error probabilities of different approaches in Trajectory III are shown in Fig. 7 and Fig. 8, respectively. The proposed MEMS solution had a RMS position error of 10.39m, which performed better than the PDR RMS position error of 45.96m. The proposed TC WiFi/MEMS integration, using all observable APs, had a RMS position error of 2.49m, which was superior to the 7.95m RMS position error of the LC integration. The improvement from LC integration to TC integration in this trajectory is much more than the other two trajectories. This is most likely because the RSS bias in the third experiment's trajectory is larger than the previous two trajectories. With the successful estimation of the large RSS bias, TC integration has a better performance than LC integration. By using two selected APs and one selected AP, TC integrations had RMS position errors of 3.12m and 4.13m, respectively. Like the other two trajectories, their navigation performance was worse than the TC integration, using all observable APs. However, they had a better navigation performance than the proposed MEMS solution. These results further illustrate the navigation performance of the proposed TC integration.

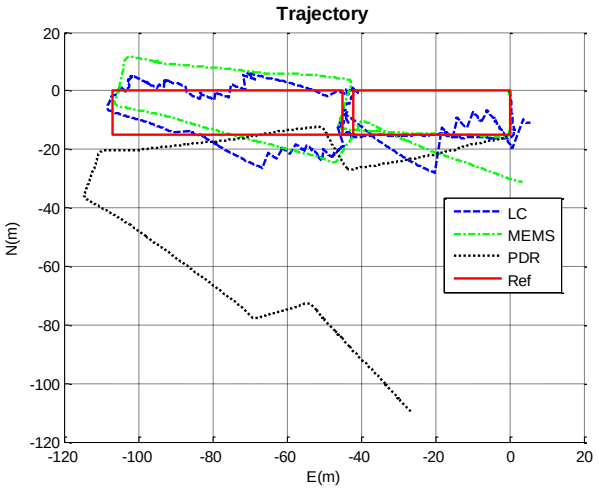

(a)

This article has been accepted for publication in a future issue of this journal, but has not been fully edited. Content may change prior to final publication. Citation information: DOI 10.1109/JSEN.2015.2477444, IEEE Sensors Journal

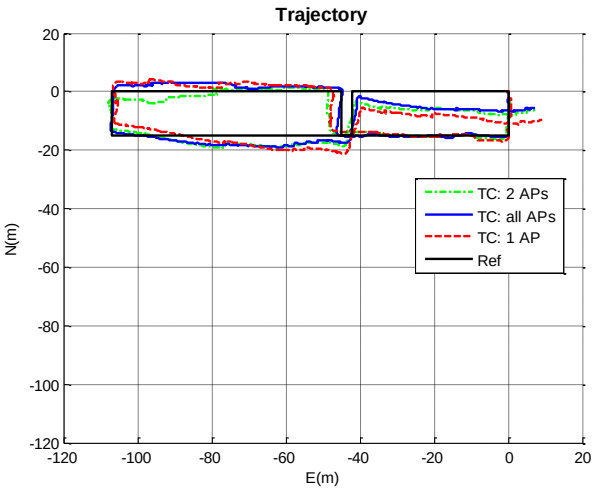

(b)

Fig. 7. Navigation solutions in Trajectory III (Pedestrian 3, Smartphone C). (a) PDR, MEMS, and WiFi/MEMS LC integration; and (b) WiFi/MEMS TC integration using different numbers of APs.

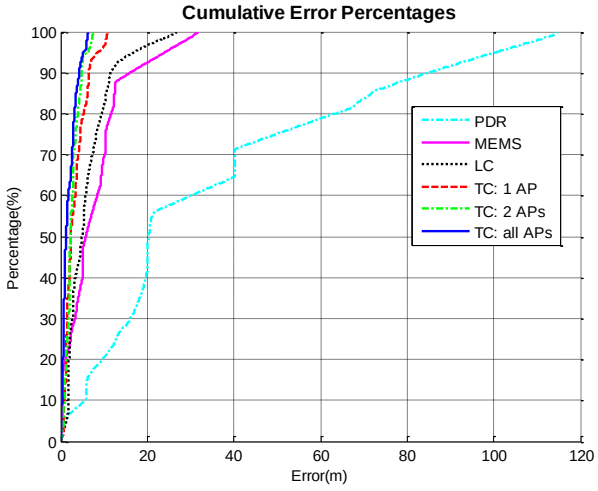

Fig. 8. Cumulative error percentages of PDR, MEMS, WiFi/MEMS LC integration and WiFi/MEMS TC integration using different numbers of APs in Trajectory III.

The navigation performance of different approaches in the three experiments are summarized in TABLE II. This table also illustrates the efficiency of the proposed indoor pedestrian navigator, based on the WiFi/MEMS TC integration. The results in TABLE II show that the average positioning error of the proposed TC integration in various trajectories is 0.01% of INS, 10.38% of PDR, 32.11% of the developed MEMS solution, and 64.58% of the LC integration.

In TABLE III, the proposed system is compared with current WiFi/MEMS integrated systems. It shows that the proposed system has slightly worse positioning accuracy when compared with [13] [14] [15]. However, these three systems are based on WiFi fingerprinting and amounted Inertial Measurement Unit (IMU). WiFi fingerprinting requires a large amount of labor and time cost for building and maintaining the radio map database. The amounted IMU is not as convenient as handheld devices for pedestrian navigation. WiFi ToF and strapped IMU are integrated in [16], and this system has the maximum positioning error of 2.5 m. However, WiFi ToF requires specially designed WiFi routers, which is not suitable for current commercial routers. For pedestrian navigation applications, the research [18] integrates propagation-model-based WiFi positioning solution with the sensor data from smartphones. Meanwhile, the research [17] uses WiFi propagation model, PDR, and multi-person collaboration to provide a positioning solution that has an accuracy of 5m (RMS). It has the worst navigation performance. However, it provides a convenient handheld navigation solution for pedestrians without building the radio map database. Our proposed system not only has this advantage, but also provides a more accurate navigation solution even in the environment with sparse deployments of WiFi APs.

TABLE II
SUMMARY OF NAVIGATION PERFORMANCE OF DIFFERENT APPROACHES

Algorithms	RMS Position Error (m)		
	T1	T2	T3
INS	13855.30	49029.47	49528.85
PDR	27.79	34.00	45.96
MEMS	10.83	11.02	10.39
LC	4.87	4.87	7.95
TC with all APs	3.72	4.19	2.49
TC with 2APs	5.77	4.36	3.12
TC with 1AP	5.87	4.44	4.13

TABLE III
COMPARED RESULT OF THE PROPOSED SYSTEM WITH CURRENT SYSTEMS

System	Algorithm	Accuracy
Proposed System	WiFi propagation model + Smartphone IMU	RMS: 3.47m
[13]	WiFi fingerprinting + Shoe IMU	RMS: 1.65m
[14]	WiFi fingerprinting + Trolley IMU	Mean: about 2.00m
[15]	WiFi fingerprinting + Shoe IMU	Mean: 1.53m
[16]	WiFi ToF + Strapped IMU	Max: 2.50m
[17]	WiFi propagation model+ Smartphone IMU + multi-person collaborative positioning	RMS: about 5.00m
[18]	WiFi propagation model + Smartphone IMU	Mean: 7.83m

VII. Conclusions and Future Work

This paper presented a handheld indoor pedestrian navigator based on the TC integration of WiFi and MEMS sensors. The main contributions of this paper are summarized as follows.

1. An indoor pedestrian navigator using a TC integration of WiFi and MEMS sensors (i.e., TC integration of WiFi, PDR, and INS) on handheld devices was originally proposed in this paper. WiFi RSS bias was introduced in the state vector for TC integration of WiFi and MEMS sensors for the first time, which improved the accuracy of the proposed system.
2. A MEMS navigation solution based on PDR/INS integration was also used to enhance the navigation performance of the indoor pedestrian navigator. Better heading is achieved by using PDR/INS integration to remove gyroscope noise which occurs if we use only vertical gyroscope. Field tests showed that the proposed MEMS solution was better than PDR and INS solutions.
3. The navigation performance of the TC integration was compared with the LC integration in indoor environment. TC

integration performs better than LC integration, especially in the environment with sparse deployment of WiFi APs.

The performance of the proposed navigation solution was illustrated to be a very competitive system for indoor pedestrian navigation. This proposed navigation solution can be used in both environments with dense and sparse deployments of WiFi APs. The method had been validated in field tests in indoor environments. Experiment results showed that the average RMS position error of the proposed TC integration solution was 3.47m in three trajectories, which is 0.01% of INS, 10.38% of PDR, 32.11% of the developed MEMS solution, and 64.58% of the LC integration. The proposed indoor pedestrian navigator can be easily implemented on most handheld devices, such as smartphones, and can contribute to the consumer electronics market.

In the future, we will use more advanced error models to further improve the accuracy of the proposed system. Furthermore, quality control algorithms will also be investigated to enhance the system robustness. Additionally, more experiments will be conducted in various environments, such as retail shops, shop floors, and offices, to evaluate the performance of the proposed system systematically.

References

[1] E. D. Kaplan and C. J. Hegarty, *Understanding GPS: principles and applications*: Artech House Publishers, 2006.

[2] Z. He, V. Renaudin, M. G. Petovello, and G. Lachapelle, "Use of High Sensitivity GNSS Receiver Doppler Measurements for Indoor Pedestrian Dead Reckoning," *Sensors*, vol. 13, pp. 4303-4326, 2013.

[3] Z. Syed, P. Aggarwal, Y. Yang, and N. El-Sheimy, "Improved Vehicle Navigation Using Aiding with Tightly Coupled Integration," in *Vehicular Technology Conference, 2008. VTC Spring 2008. IEEE*, 2008, pp. 3077-3081.

[4] Z. Lei, L. Jiangchuan, J. Hongbo, and G. Yong, "SensTrack: Energy-Efficient Location Tracking With Smartphone Sensors," *Sensors Journal, IEEE*, vol. 13, pp. 3775-3784, 2013.

[5] W. Dae Hee, L. Eunsung, H. Moonbeom, L. Seung-Woo, L. Jiyun, K. Jeongrae, *et al.*, "Selective Integration of GNSS, Vision Sensor, and INS Using Weighted DOP Under GNSS-Challenged Environments," *Instrumentation and Measurement, IEEE Transactions on*, vol. 63, pp. 2288-2298, 2014.

[6] Y. Zhuang, Z. Syed, J. Georgy, and N. El-Sheimy, "Autonomous smartphone-based WiFi positioning system by using access points localization and crowdsourcing," *Pervasive and Mobile Computing*, vol. 18, pp. 118-136, 2015.

[7] H. Lan, C. Yu, Y. Zhuang, Y. Li, and N. El-Sheimy, "A State Constraint Kalman Filter for Pedestrian Navigation with Low Cost MEMS Inertial Sensors," in *Proceedings of the 28th International Technical Meeting of The Satellite Division of the Institute of Navigation (ION GNSS+ 2015)*, Tampa, FL, USA, 2015.

[8] Y. Li, Y. Zhuang, H. Lan, P. Zhang, X. Niu, and N. El-Sheimy, "WiFi-Aided Magnetic Matching for Indoor Navigation with Consumer Portable Devices," *Micromachines*, vol. 6, p. 747, 2015.

[9] C. Lyu-Han, E. H. K. Wu, J. Ming-Hui, and C. Gen-Huey, "Homogeneous Features Utilization to Address the Device Heterogeneity Problem in Fingerprint Localization," *Sensors Journal, IEEE*, vol. 14, pp. 998-1005, 2014.

[10] Y. Zhuang, H. Lan, Y. Li, and N. El-Sheimy, "PDR/INS/WiFi Integration Based on Handheld Devices for Indoor Pedestrian Navigation," *Micromachines*, vol. 6, p. 793, 2015.

[11] P. Aggarwal, Z. Syed, and N. El-Sheimy, *MEMS-Based Integrated Navigation*: Artech House 2010.

[12] A. J. Ruiz, F. S. Granja, J. C. Prieto Honorato, and J. I. Rosas, "Accurate Pedestrian Indoor Navigation by Tightly Coupling Foot-Mounted IMU and RFID Measurements," *Instrumentation and Measurement, IEEE Transactions on*, vol. 61, pp. 178-189, 2012.

[13] K. Frank, B. Krach, N. Catterall, and P. Robertson, "Development and evaluation of a combined wlan & inertial indoor pedestrian positioning system," in *ION GNSS*, 2009.

[14] X. Wendong, N. Wei, and T. Yue Khing, "Integrated Wi-Fi fingerprinting and inertial sensing for indoor positioning," in *Indoor Positioning and Indoor Navigation (IPIN), 2011 International Conference on*, 2011, pp. 1-6.

[15] F. Evennou and F. Marx, "Advanced integration of WiFi and inertial navigation systems for indoor mobile positioning," *Eurasip journal on applied signal processing*, vol. 2006, pp. 164-164, 2006.

[16] U. Schatzberg, L. Banin, and Y. Amizur, "Enhanced WiFi ToF indoor positioning system with MEMS-based INS and pedometric information," in *Position, Location and Navigation Symposium - PLANS 2014, 2014 IEEE/ION*, 2014, pp. 185-192.

[17] T. Iwase and R. Shibasaki, "Infra-free indoor positioning using only smartphone sensors," in *Indoor Positioning and Indoor Navigation (IPIN), 2013 International Conference on*, 2013, pp. 1-8.

[18] W. W.-L. Li, R. Iltis, and M. Z. Win, "A smartphone localization algorithm using RSSI and inertial sensor measurement fusion," in *Global Communications Conference (GLOBECOM), 2013 IEEE*, 2013, pp. 3335-3340.

[19] Y. Yi and D. Grejner-Brzezinska, "Tightly-coupled GPS/INS integration using unscented Kalman filter and particle filter," in *Proceedings of the 19th International Technical Meeting of the Satellite Division of The Institute of Navigation (ION GNSS 2006)*, 2006, pp. 2182-2191.

[20] Y. Li, J. Wang, C. Rizos, P. Mumford, and W. Ding, "Low-cost tightly coupled GPS/INS integration based on a nonlinear Kalman filtering design," in *Proceedings of ION National Technical Meeting*, 2006, pp. 18-20.

[21] M. George and S. Sukkarieh, "Tightly coupled INS/GPS with bias estimation for UAV applications," in *Proceedings of Australiasian Conference on Robotics and Automation (ACRA)*, 2005.

[22] J. Wendel and G. F. Trommer, "Tightly coupled GPS/INS integration for missile applications," *Aerospace Science and Technology*, vol. 8, pp. 627-634, 2004.

[23] M. Morgado, P. Oliveira, C. Silvestre, and J. F. Vasconcelos, "USBL/INS Tightly-Coupled Integration Technique for Underwater Vehicles," in *Information Fusion, 2006 9th International Conference on*, 2006, pp. 1-8.

[24] D. H. Titterton and J. L. Weston, "Strapdown Inertial Navigation Technology (2nd Edition)," ed: Institution of Engineering and Technology, 2004.

[25] H. Chengliang, L. Zaiyi, and Z. Lian, "Synergism of INS and PDR in Self-Contained Pedestrian Tracking With a Miniature Sensor Module," *Sensors Journal, IEEE*, vol. 10, pp. 1349-1359, 2010.

[26] Y. Li, J. Georgy, X. Niu, Q. Li, and N. El-Sheimy, "Autonomous Calibration of MEMS Gyros in Consumer Portable Devices," *IEEE Sensors Journal*, vol. 15, pp. 4062-72, 2015.

[27] R. Harle, "A survey of indoor inertial positioning systems for pedestrians," *IEEE Communications Surveys and Tutorials*, vol. 15, pp. 1281-1293, 2013.

[28] H. Weinberg, "Using the ADXL202 in pedometer and personal navigation applications," *Analog Devices AN-602 application note*, 2002.

[29] A. Gelb, *Applied optimal estimation*: MIT Press, 1999.

[30] X. Niu, Y. Li, H. Zhang, Q. Wang, and Y. Ban, "Fast Thermal Calibration of Low-Grade Inertial Sensors and Inertial Measurement Units," *Sensors*, vol. 13, pp. 12192-12217, 2013.

[31] N. El-Sheimy, "Inertial Techniques and INS/DGPS Integration," Department of Geomatics Engineering, University of Calgary, Calgary, Canada 2006.

[32] Z. Xiao, H. Wen, A. Markham, and N. Trigoni, "Robust pedestrian dead reckoning (R-PDR) for arbitrary mobile device placement," in *International Conference on Indoor Positioning and Indoor Navigation*, 2014, p. 30th.

[33] S. Mazuelas, A. Bahillo, R. M. Lorenzo, P. Fernandez, F. A. Lago, E. Garcia, *et al.*, "Robust indoor positioning provided by real-time RSSI values in unmodified WLAN networks," *Selected Topics in Signal Processing, IEEE Journal of*, vol. 3, pp. 821-831, 2009.

[34] J. Salo, L. Vuokko, H. M. El-Sallabi, and P. Vainikainen, "An Additive Model as a Physical Basis for Shadow Fading," *Vehicular Technology, IEEE Transactions on*, vol. 56, pp. 13-26, 2007.

[35] P. Bahl and V. N. Padmanabhan, "RADAR: an in-building RF-based user location and tracking system," in *INFOCOM 2000. Nineteenth Annual Joint Conference of the IEEE Computer and Communications Societies. Proceedings. IEEE*, 2000, pp. 775-784 vol.2.

[36] M. Lott and I. Forkel, "A multi-wall-and-floor model for indoor radio propagation," in *Vehicular Technology Conference, 2001. VTC 2001 Spring. IEEE VTS 53rd*, 2001, pp. 464-468 vol.1.